Two-stage Multi-objective Optimization Coordination of Electro-thermal Coupled Integrated Energy System Based on Improved NSGA-II Algorithm

Na Zhang[1,*] and Taozhu Feng[2]

[1]*School of Management, Xi' an University of Science and Technology, 710054, China*
[2]*Center for Energy Economy and Management Research, Xi' an University of Science and Technology, 710054, China*
E-mail: 20202097035@stu.xust.edu.cn
[*]*Corresponding Author*

Received 17 March 2023; Accepted 13 April 2023;
Publication 26 August 2023

Abstract

With the growing proportion of clean energy in integrated energy systems (IES), energy supply uncertainty and spatial-temporal dispersion are becoming increasingly prevalent. System modeling and optimal scheduling are facing greater challenges. In this paper, we improve the non-dominated sorting genetic algorithm (NSGA-II) to address the above problems and propose a two-stage multi-objective benefit-equilibrium optimization coordination of the electric-thermal coupled integrated energy system. Firstly, this paper carries out the thermodynamic characteristics analysis of the equipment components of the electro-thermal coupled energy system, which reflects the structural features of the system, the performance of each equipment under different task conditions, and the mechanism of the system; based on the above characteristic analysis, a two-stage multi-objective optimization of electro-thermal coupled system optimization coordination is proposed

Distributed Generation & Alternative Energy Journal, Vol. 38_6, 1707–1740.
doi: 10.13052/dgaej2156-3306.3861
© 2023 River Publishers

to establish the objective function and carry out each objective balance constraint; the NSGA-II algorithm is as well as improved. According to the operation stage, operation generation and the NSGA-II algorithm are improved by dynamically adjusting the operating parameters of evolving individuals of the operation stage, operational generation, and the number of undominated individuals in the current temporary population. By making the algorithm adaptation to improve the adaptive capacity of the evolution operator, we solve the two-step model and obtain the Pareto optimal front for each energy device. In summary, the results of the analysis of the IES under the coupling of power system and thermal system show that the constructed model and the proposed algorithm can effectively improve the accuracy of the renewable energy system and the optimization decision. The results of the research further reflect the benefits of the proposed multi-objective optimization scheme in accounting for economic, renewable energy, and complex operating constraints which ensure the economical and stable operation of the system, as well as the robustness of optimal scheduling.

Keywords: Integrated energy system, electric-thermal coupling, multi-objective optimization, benefit equilibrium, NSGA-II algorithm.

1 Introduction

As an effective means to coordinate the planning and optimal dispatch of multiple forms of energy supply, integrated energy systems (IES) can use controllable power supply units within the system to smooth out the uncertainty of clean energy, thus energy efficiency can be improved. We also reduce the wastage of resources caused by wind and stray light to meet user demand for an eco-friendly energy system. By 2030, China plans to reach peak carbon emissions, and by 2060, it plans to achieve carbon neutrality [1]. The ambitious carbon neutrality targets of 2030 and 2060 have been met. Currently, there has been a great deal of research into integrated energy use by academics at home and abroad, which can be broadly divided into two aspects: modeling and optimal scheduling. The first focuses on application scenarios, hardware structures, and energy supply uncertainty analysis. The second focuses on optimization algorithms and scheduling on multiple timescales. Unfortunately, these studies tend to ignore the equipment's varying operating characteristics, but the energy conversion efficiency by default is still the nominal value. While this simplification may reduce the difficulty of modeling, it can lead to a shift in the energy conversion relationship

of the system and the accuracy of optimal scheduling results, especially under low-load conditions [2]. Furthermore, IES also implies coordinated complementarity of multiple energy sources. Deviations caused by neglecting the varying operating condition characteristics of individual multi-energy cogeneration equipment can be transferred to the overall system with the energy coupling relation. For this reason, it is essential to set up a machine mannequin that can mirror the traits of various running prerequisites in order to make the sure protected operation of the machine and meet the necessities of sensible functions [3].

Currently, Bayu A et al. used solar PV combined with wind turbines to generate electricity and the developed hybrid system was connected to the grid to supply the load, by modeling the components of the power network and hybrid power network using MATLAB software [4]; Huang Zonghong et al. proposed an energy management method for integrated energy systems considering the reliability of energy supply for the poor coordination and economic energy management in existing industrial parks [5]; Gireesh V. Puthusserry et al. proposes an improved genetic algorithm (GA) for maximum power point tracking (MPPT) in shaded photovoltaic power generation systems, where healthier chromosomes are retained for the next generation and poorly performing chromosomes are sequentially removed from the population [6]; Zhang T et al. used a typical scenario set to consider the uncertainty of wind power output and established a regionally integrated energy system optimal dispatch model, which utilized a non-dominated ranking genetic algorithm (NSGA-II) to solve and output the Pareto optimal frontier solution set [7]; Prakash S N et al. achieve optimal dispatch of the proposed generating units by economic/environmental power dispatch to reduce the total operating cost and net emissions of the system while considering the effects of grid-connected and autonomous operation modes and satisfying operational constraints [8].

Embedded energy systems are becoming cleaner and energy-orientated, and energy supply uncertainty, and spatial and temporal dispersion are becoming increasingly prevalent. System modeling and optimal scheduling are facing greater challenges. In this paper, we improve on the undominated sorting genetic algorithm to address the above problems and propose a two-stage multi-objective coordination of benefit-balanced optimization for embedded energy systems. First, this paper performs the analysis of the thermodynamic characteristics of the equipment components of the integrated power system, which reflects the structural features of the system, the operating performance of each equipment under different working conditions,

and the operating mechanism of the system; based totally on the above function analysis, coordination of the electricity device optimization built-in with two-stage multi-objective optimization is proposed to set the goal characteristic and understand the stability constraint of every objective; the NSGA-II algorithm is improved, and in accordance to the operation stage, operation technology and The NSGA-II algorithm is multiplied by way of dynamically adjusting the running parameters of evolving men and women in accordance to the operation stage, the technology of operations and the quantity of undominated men and women in the modern-day brief population, via making the algorithm adaptive via enhancing the adaptive capability of the evolutionary operator, fixing the two stage model, and acquiring the Pareto ideal the front for every power device. In summary, the effects of the algorithm evaluation exhibit that the built mannequin and the proposed algorithm can efficiently enhance the accuracy of the renewable electricity machine and the optimization decision. The consequences of the lookup in addition mirror the advantages of the proposed multi-objective optimization scheme in accounting for economic, renewable strength and complicated working constraints to make certain within your budget and steady operation of the system, as nicely as the robustness of gold standard scheduling.

2 Thermodynamic Characterization of Integrated Energy System Equipment Components

2.1 Thermodynamic Characteristics of a Typical Natural Gas Combined Cooling, Heating, and Power System

(a) Engine

Natural gas Combined Cooling, Heating and Power (CCHP) systems usually use gas turbines, the role of internal combustion engines and micro combustion engines in transportation. Among all types of prime movers, gas turbine and internal combustion engine technologies are more mature, and these are the most widely used technologies in distributed electricity systems. The gas turbine is the primary research focus of this paper, and the capacity of gas turbines common in CCHP systems varies from several hundred kilowatts to as much as 50 MW, which mainly has the following characteristics: waste heat recovery in the form of steam; low vibration, no need for special anti-vibration facilities [9]; can select gas or liquid fuel and can use water injection, steam injection, and other low NOx burning technologies; output power is subject to environmental conditions The output power

is influenced by environmental conditions (temperature, pressure, etc.); it has low power generation efficiency but high waste heat, and waste heat can easily be recovered without the need for cooling water; equipment operation and maintenance costs are low.

According to the structure and operation principle of the compressor, its thermodynamic characteristics are modeled as follows.

Compressor outlet air pressure:

$$P_2 = \pi_c * P_1 \tag{1}$$

Compressor outlet temperature:

$$T_2 = T_1 \left[1 + \left(\pi^{\frac{k_a-1}{k_n}} - 1\right) \Big/ \eta_c\right] \tag{2}$$

Compressor power consumption:

$$N_c = G_c C_{pct} T_1 \left(\pi_c^{\frac{k_{tu}-1}{k_{at}}} - 1\right) \Big/ \eta_c \tag{3}$$

The compressor efficiency can be obtained:

$$\eta_c = w_1 / w_2 \tag{4}$$

Where w_1 is the effective work obtained by air:

$$w_1 = \frac{k_a}{k_a - 1} R_g T_a \left(\pi_c^{\frac{k_a-1}{k_a}} - 1\right) \tag{5}$$

w_2 is the effective work delivered to the air by the impeller:

$$w_2 = T_{20}^2(\mu + f_0 - cT_0/T_{20}^2) \tag{6}$$

$$\pi_c = \dot{\pi}_c * \pi_{c0} \tag{7}$$

$$\dot{\pi}_c = C_1(\dot{n})\dot{G}_c^2 + C_2(\dot{n})\dot{G}_c^2 + C_3(\dot{n}) \tag{8}$$

$$\dot{n} = n/\sqrt{T_1} \tag{9}$$

$$\dot{G}_c = G_c\sqrt{T_1}/P_1 \tag{10}$$

To model the thermodynamics of the combustion chamber, we first assume that the losses of air resistance and gas flow are not considered [10], i.e. $G_{a,in} = G_{a,owu}$, $G_{omt} = G_{a,out} + G_r$, where Gr is the natural gas consumption.

Combustion chamber outlet temperature:

$$T_3 = \frac{C_{pu} G_{a,out} T_2 + G_r (q_r \eta_B + h_r)}{C_{pg} G_{out}} \tag{11}$$

In order for a turbine to operate correctly, it has to have low turbine outlet temperatures and high turbine drive powers.

Turbine outlet temperature:

$$T_4 = T_3 \left[1 - \left(1 - \frac{1}{\pi^{\frac{k_x - 1}{k_x}}} \right) \eta_1 \right] \tag{12}$$

Turbine drive power:

$$N_1 = G_1 C_{pg} T_3 \left(1 - \frac{1}{\pi_l \frac{k_x - 1}{k_x}} \right) \eta_1 \tag{13}$$

Assuming no mechanical loss of power, the mathematical model of the rotor is as follows:

$$J \frac{d\omega}{dt} = M_t - M_{\mathrm{c}} - M_m - M_l \tag{14}$$

Since $\omega = \frac{2\pi n}{60}$, $N = \frac{M}{\omega}$, and thus

$$\frac{dn}{dt} = \frac{900}{J \pi^2 n} (N_1 - N_c - N_m - N_l) \tag{15}$$

As shown in the following diagram, the generator has the following thermodynamic model:

$$M_f = \frac{9555 N_{out}}{n} \tag{16}$$

Then the efficiency of the whole gas turbine generator set is:

$$\eta = \frac{N_{out}}{Q_{nk}^{gt}} = \frac{N_{out}}{G_r (q_r \eta_B + h_r)} \tag{17}$$

So that it accurately reflects the actual operating characteristics of different equipment sizes under varying operating conditions, in order to obtain the thermal value of the gas turbine exhaust available, test data from equipment manufacturers are fitted [11].

$$Q_{fg,t} = p_{gt} Q_{ng}^{gt} + q_{gt} \tag{18}$$

The full-load generation capacity with respect to the temperature correction model is as follows:

$$CAP_{gt,r} = CAP_{gt,r0}[1 - c_{gt}((t_{gt} - t_{gt,0}) + |t_{gt} - t_{gt,0}|)/2] \tag{19}$$

where, p_{gt}, q_{gt}, c_{gt} is the fitting coefficient

(b) Boiler

A boiler's heating efficiency is primarily determined by its partial load rate, which has the following relationship with its thermal efficiency:

$$\eta_{b,1} = \eta_{b,r}(0.0951 + 1.525PLR_{b,t} - 0.6249PLR_{b,t}^2) \tag{20}$$

For waste heat and gas boilers, the relationship between part load flow and thermal efficiency is usually the best performance when the boiler is maintaining an operating load of 85%–100% of the full load. And when its load is less than 80% or greater than 100% the thermal efficiency of the boiler tends to decrease quickly.

(c) Absorption chillers

In this study, a lithium bromide dual-effect absorption chiller is used, which directly uses the heat allocated to the absorption chiller by the gas turbine and the solar collector as the driving heat source [12].

The thermodynamic modeling of absorption chillers used in this study is based on the DOE-2 chiller model in ASHRAE Standard 90.1. The factors that affect the time-by-time cooling efficiency of absorption chillers are the time-by-time chilled water outlet temperature, the time-by-time cooling water inlet temperature, and the time-by-time part-load rate.

The following three equations are used to express the capacity correction factor and absorption refrigerator cooling power correction factor as a function of temperature and part load rate at different operating conditions.

Temperature-to-capacity correction factor:

$$\begin{aligned}\mathrm{CAPCF}_{ac,t} = {} & a_1 + b_1 \times T_{ac\cdot wo,t} + c_1 \times T_{ac,wo,t}^2 + d_1 \times T_{ac,cr,t} \\ & + e_1 \times T_{ac,cr,t}^2 + f_1 \times T_{ac,wo,t} \times T_{ac,ci,t}\end{aligned} \tag{21}$$

Temperature to cooling power correction factor:

$$\begin{aligned}\mathrm{EIRCF}_{ac,t} = {} & a_2 + b_2 \times T_{ac,wo,t} + c_2 \times T_{ac,wo,t}^2 + d_2 \times T_{ac,cr,t} \\ & + e_2 \times T_{ac,cr,t}^2 + f_2 \times T_{ac,wo,t} \times T_{ac,ci,t}\end{aligned} \tag{22}$$

Partial load rate to cooling power correction factor:

$$PLRCF_{ac,t} = a_3 + b_3 \times PLR_{ac,t} + c_3 \times PLR_{ac,l}^2 + d_3 \times PLR_{ac,t}^3 \quad (23)$$

The modified hour-by-hour capacity of the absorption chiller is as follows:

$$CAP_{ac,t} = CAP_{ac,0} \times CAPCF_{ac,t} \quad (24)$$

Among them, the hour-by-hour load rate of absorption chillers:

$$PLR_{ac,t} = \frac{Q_{ac,t}^{load}}{CAP_{ac,t}} \quad (25)$$

Where, $Q_{ac,t}^{load}$ is the hour-by-hour load of the absorption chiller, gas turbines, and solar thermal systems contribute approximately equal amounts of heat to the absorption chiller.

Then the hour-by-hour cooling capacity of the absorption refrigerator is:

$$Q_{ac,t} = Q_{ac,r} \times CAPCF_{ac,t} \times EIRCF_{ac,t} \times PLRCF_{ac,t} \quad (26)$$

$$Q_{ac,r} = CAP_{ac,0} \times COP_{ac,0} \quad (27)$$

Where a∼f are the correlation coefficients derived from the DOE-2 model fitted with actual data.

(d) Electric refrigeration

Electric compression refrigerators (hereinafter referred to as cr) and lithium bromide absorption chillers belong to the same chiller, so the DOE-2 chiller model can still be used for the simulation of capacity, energy efficiency, and load performance, as follows:

$$\begin{cases} CAPCFF_{cr,t} = a_4 + b_4 \times T_{cr,wo,t} + c_4 \times T_{cr,wo,t}^2 + d_4 \times T_{cr,ci,t} \\ \qquad\qquad + e_3 \times T_{cr,ci,t}^2 + f_3 \times T_{cr,wo,t} \times T_{cr,ci,t} \\ COPCFF_{cr,t} = a_5 + b_5 \times T_{cr,wo,t} + c_5 \times T_{cr,wo,t}^2 + d_5 \times T_{cr,ci,t} \\ \qquad\qquad + e_4 \times T_{cr,ci,t}^2 + f_4 \times T_{cr,wo,t} \times T_{cr,ci,t} \\ PLRCF_{cr,t} = a_6 + b_6 \times PLR_{cr,t} + c_6 \times PLR_{cr,t}^2 + d_6 \times PLR_{cr,t}^3 \end{cases} \quad (28)$$

Then there are.

$$\begin{cases} CAP_{cr,t} = CAP_{cr,0} \times CAPCF_{cr,t} \\ PLR_{cr,t} = Q_{cr,t}^{load} / CAP_{cr,t} \\ Q_{cr,r} = CAP_{cr,0} \times COP_{cr,0} \end{cases} \quad (29)$$

Where, $Q_{cr,t}^{load}$ is the hourly load of the electric chiller, which is approximately equal to the hourly power consumption of the electric chiller $E_{cr,t}$.

So here is the actual operating power of the electric chiller:

$$Q_{cr,t} = Q_{cr,r} \times CAPCF_{cr,t} \times EIRCF_{cr,t} \times PLRCF_{cr,t} \tag{30}$$

In this study case, we take the electric chiller not to run in winter in our decision due to the small cold and hot compress in winter.

2.2 Thermodynamic Characteristics of a Typical Solar System

Solar power resources are widely used in embedded energy systems due to their cleanliness, prevalence, abundance, and low cost of operation and maintenance [13]. Solar power systems primarily consist of solar photovoltaics (PV) (hereafter referred to as PV systems) and solar thermal power systems (hereafter referred to as ST systems).

(a) Photovoltaic power generation system

The hour-by-hour electricity era of PV strength machines is on the whole affected by the parameters such as photo voltaic radiation depth and PV telephone set temperature. The thermodynamic mannequin of the PV electricity era gadget is as follows.

The hour-by-hour power generation capacity of the solar photovoltaic system is:

$$E_{pv,t} = A_{pv} \times \eta_{pv,t} \times SRI_t \tag{31}$$

The hour-by-hour power generation efficiency of the photovoltaic cell system is:

$$\eta_{pv,t} = \eta_{T_{ref}}[1 - \beta_{ref}(T_{c,t} - T_{ref})] \tag{32}$$

$$\beta_{ref} = \frac{1}{T_0 - T_{ref}} \tag{33}$$

Where, T_o is the temperature when the electrical efficiency of the PV cell set is 0, and 270°C for crystalline silicon cells. T_c is the operating temperature of the PV cell, i.e.:

$$T_{c,t} = T_{a,t} + (T_{nor} - 20)\frac{SRI_t}{800} \tag{34}$$

where, refers to the rated running cellphone temperature, described as the mobile temperature measured underneath open-circuit stipulations at an

ambient temperature of 20°C, radiation depth of 800 W/m^2, and wind velocity of 1 m/s.

(b) Solar Thermal Systems

In a typical solar thermal system, the basic structure consists primarily of solar collectors, absorber refrigeration units, and other ancillary equipment such as heat exchangers [14]. One of these is the absorption refrigeration unit which is responsible for converting the heat generated in the solar collector into an effective cooling load in order to provide cooling to the user; it is the responsibility of the heat exchanger to convert the heat in the solar collector into an effective heat load to provide heat to the user. Here is the thermodynamic model around the solar collector.

$$Q_{st,t} = A_{st} \times \eta_{st,t} \times SRI_t \tag{35}$$

Where, $\eta_{st,t}$ is the time-by-time solar collector heating efficiency, its size depends on the average temperature $T_{f.t}$ of the fluid in the collector tube, time-by-time ambient temperature $T_{a,t}$ and tilted surface time-by-time solar radiation SRI_t, that is:

$$\eta_{st,t} = \eta_{opt} K_{\theta,t} - a_1 \times \frac{T_{f,t} - T_{a,t}}{SRI_t} - a_2 \times \frac{(T_{f,t} - T_{a,t})^2}{SRI_t} \tag{36}$$

where, *temperature and global heat loss coefficient are correlated by* a_1, a_2, taking $a_1 = 1.26, a_2 = 0.004$; $K_{\theta,t}$ are the correction coefficients of time-by-time solar incidence angle, i.e.:

$$\theta_{l,t} = |\tan^{-1}(\tan\theta_z \cos(\gamma - \gamma_s)) - \beta| \tag{37}$$

$$\theta_{tr,t} = \left|\tan^{-1}\left(\frac{\sin\theta_z \sin(\gamma - \gamma_s)}{\cos\theta}\right)\right| \tag{38}$$

2.3 Air Source Heat Pump

Air source heat pumps are responsible for converting heat from the air that cannot be directly utilized (low level heat source) into high level heat energy for indoor heating. The air source heat pump unit mainly consists of a compressor, condensing heat exchanger, expansion valve, evaporating heat exchanger and compressor.

Since the heat pump operates under partial load conditions most of the time, the focus of the simulation study of the heat pump system in this paper is

the performance of the heat pump unit working under partial load conditions, and the variable operating mechanism of the heat pump is the same as that of the refrigeration unit, so the same DOE-2 model is used for the simulation analysis of the air source heat pump. The mathematical model is as follows:

$$\begin{cases} CAPCF_{\mathrm{ashp},t} = a_7 + b_7 \times T_{\mathrm{ashp,wo,t}} + c_7 \times T^2_{\mathrm{ashp,wo,t}} + d_7 \times T_{\mathrm{ashp,ci,t}} \\ \qquad\qquad + e_5 \times T^2_{\mathrm{ashp,ci,t}} + f_5 \times T_{\mathrm{ashp,wo,t}} \times T_{\mathrm{ashp,ci,t}} \\ COPCF_{\mathrm{askp},t} = a_8 + b_8 \times T_{\mathrm{ashp,wo,t}} + c_8 \times T^2_{\mathrm{ashp,wo,t}} + d_8 \times T_{\mathrm{ashp,ci,t}} \\ \qquad\qquad + e_6 \times T^2_{\mathrm{ashp},ci,t} + f_6 \times T_{\mathrm{ashp,wo,t}} \times T_{\mathrm{ashp,ci,t}} \\ PLRCF_{\mathrm{ashp},t} = a_9 + b_9 \times PLR_{\mathrm{ashp},t} + c_9 \times PLR^2_{\mathrm{ashp},t} \\ \qquad\qquad + d_9 \times PLR^3_{\mathrm{ashp},t} \end{cases} \tag{39}$$

From the above, it follows that

$$\begin{cases} CAP_{\,ashp,t} = CAP_{\,ashp,0} \times CAPCF_{\,ashp,t} \\ PLR_{ashp,t} = Q^{load}_{ashp,t} / CAP_{\,ashp,t} \\ Q_{\,ashp,r} = CAP_{\,ashp,0} \times COP_{\,ashp,0} \end{cases} \tag{40}$$

Then the hour-by-hour heat production efficiency of the air source heat pump is

$$Q_{\,ashp,t} = Q_{\,ashp,r} \times CAPCF_{\,ashp,t} \times EIRCF_{\,ashp,t} \times PLRCF_{\,ashp,t} \tag{41}$$

3 Two-Stage Multi-objective Optimization Model

The block logic diagram for the two-stage multi-objective optimal allocation approach is shown in Figure 1. In the first stage planning model, the optimal economic cost and the lowest CO_2 emissions in the life cycle are taken as objective functions, economic parameters for all equipment, machine running parameters and outcomes from the 2d stage optimization mannequin as input, and most beneficial gear kind and functionality as output [15]. In the 2d stage optimization model, the lowest working fee of the gadget is taken as the optimization goal, technical parameters for all equipment, energy prices, and results from the first stage optimization model as inputs. Using this strategy, the system's computation efficiency can be improved and the operating costs can be reduced. For improving the system's efficiency and reducing the system's running time, we choose the typical daily data instead of annual

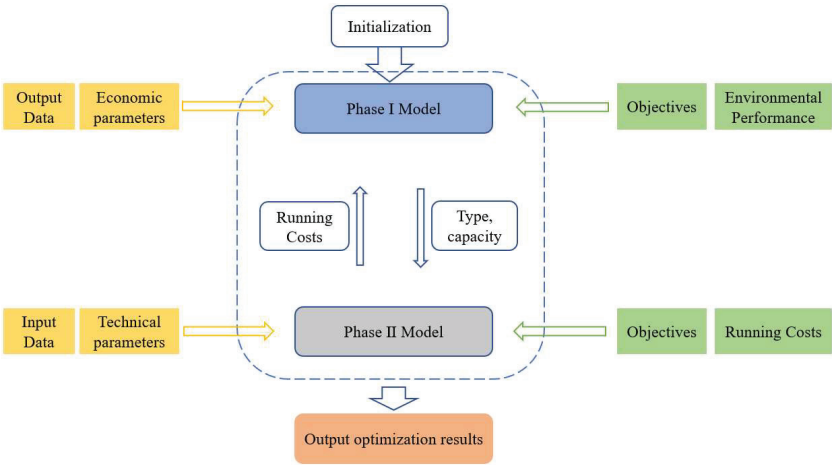

Figure 1 Two-stage optimization method.

data for the optimal design of the embedded energy system during the second stage optimization run [16].

3.1 Phase I Optimization Model

Minimizing the objective function involves minimizing the total present value of the system components during its life cycle, which is expressed as follows:

$$CRF(l,r) = \frac{r \cdot (1+\mathrm{r})^l}{(1+\mathrm{r})^l - 1} \tag{42}$$

Total annualized cost includes investment cost and operating cost per unit

$$C^{TAAN} = ZIC + ZOC \tag{43}$$

where, *ZIC* and *ZOC* are the initial construction investment cost and operating cost, respectively, ¥. The calculation method is

$$ZIC = \sum_{m \in CHP} IC_{\mathrm{m}}^{\mathrm{CHP}} + \sum_{n \in W} IC_{\mathrm{n}}^{\mathrm{Whnd}} + \sum_{i \in B} IC_{i}^{\mathrm{Bdieer}} + \sum_{j \in E} IC_{j}^{\mathrm{ES}} + \sum_{h \in T} IC_{h}^{\mathrm{TS}} + \sum_{v \in A} IC_{v}^{\mathrm{AC}} \tag{44}$$

Where, *m, n, i, j, h, v* are the serial numbers of CHP units, photovoltaic units, boiler units, electric storage equipment, thermal storage tanks, and absorption chillers, $IC_{\mathrm{m}}^{\mathrm{CHP}}, IC_{\mathrm{n}}^{\mathrm{Wind}}, IC_{i}^{\mathrm{Bolier}}, IC_{j}^{\mathrm{ES}}, IC_{h}^{\mathrm{TS}}$ are

the installation costs of CHP units, wind turbine installation costs, boiler unit installation costs, electric storage installation costs, and thermal storage installation costs, respectively, ¥.

$$ZOC = \sum_{\mathrm{t}\in NT} OC_{\mathrm{m},s,\mathrm{t}}^{\mathrm{CHP}} + \sum_{t\in NT} OC_{i,s,t}^{\mathrm{Bolier}} + \sum_{t\in NT} O_{s,t}^{\mathrm{Crid}} \tag{45}$$

where, $OC_{\mathrm{m,s,t}}^{\mathrm{CHP}}, OC_{i,s,t}^{\mathrm{Bolier}}, OC_{\mathrm{s,t}}^{\mathrm{Gid}}$ are the operating costs of CHP units, boiler unit operating costs, and network operating costs, respectively, ¥.

$$IC_{\mathrm{m}}^{\mathrm{CHP}} = CC_{m}^{\mathrm{CHP}} \cdot P_{i}^{\mathrm{CHP,Max}} \times I_m \tag{46}$$

$$IC_{\mathrm{n}}^{\mathrm{Wind}} = CC_{n}^{\mathrm{Wind}} \cdot I_n \tag{47}$$

$$IC_{i}^{\mathrm{Bolier}} = CC_{i}^{\mathrm{Bolier}} \cdot H_{i}^{\mathrm{Bolier,Max}} \cdot I_i \tag{48}$$

$$IC_{v}^{\mathrm{AC}} = CC_{v}^{\mathrm{AC}} \cdot C_{v}^{\mathrm{AC,Max}} \cdot I_v \tag{49}$$

$$IC_{j}^{\mathrm{ES}} = CC_{\mathrm{j}}^{\mathrm{ES}} \cdot E_{\mathrm{Max}} \cdot I_j \tag{50}$$

$$IC_{h}^{\mathrm{TS}} = CC_{h}^{\mathrm{TS}} \cdot E_{\mathrm{Max}} \cdot I_h \tag{51}$$

where, $CC_{m}^{\mathrm{CHP}}, CC_{n}^{\mathrm{Wind}}, CC_{\mathrm{i}}^{\mathrm{Bolier}}, CC_{v}^{\mathrm{AC}}, CC_{\mathrm{j}}^{\mathrm{ES}}, CC_{h}^{\mathrm{TS}}$ are the capital construction cost of CHP unit, wind turbine, gas boiler, absorption chiller, electric energy storage, and thermal energy storage, respectively, ¥; $I_m, I_n, I_i, I_v, I_j, I_h$ are the binary variables of whether CHP unit, photovoltaic unit, gas boiler, absorption chiller, electric energy storage and thermal energy storage are invested in construction or not, with 1 for investment in construction and 0 otherwise; $P_{i}^{\mathrm{CHP,Max}}$ is the upper limit of CHP generation capacity, *kW*; $H_{i}^{\mathrm{Bolier,Max}}$ is the upper limit of heat production of gas boiler, *kW*; $C_{v}^{\mathrm{AC,Max}}$ is the upper limit of the cooling capacity of an absorption chiller, *kW*. E_{Max} is the upper limit of energy storage, *kW•h*.

$$OC_{m,t}^{\mathrm{CHP}} = FC_{\mathrm{m},t}^{\mathrm{CHP}} + P_{m,t}^{\mathrm{CHP}} \cdot CM_{m}^{\mathrm{CHP}} \tag{52}$$

$$OC_{i,t}^{\mathrm{Boiler}} = FC_{j,t}^{\mathrm{Boiler}} + H_{j,t}^{\mathrm{Boiler}} \cdot CM_{j}^{\mathrm{Boiler}} \tag{53}$$

$$OC_{t}^{\mathrm{Grid}} = GB_t - GS_t \tag{54}$$

Where, $FC_{m,t}^{\mathrm{CHP}}, FC_{j,t}^{\mathrm{Boiler}}$ are the fuel cost of cogeneration units and gas boilers, respectively, ¥/m^3; $P_{m,t}^{CHP}, H_{j,t}^{\mathrm{Boiler}}$ are the capacity of cogeneration units and gas boilers, respectively, *kW*; $CM_{m}^{\mathrm{CHP}}, CM_{j}^{\mathrm{Boiler}}$ are the

maintenance factor of cogeneration units and gas boilers, respectively. GB_t and GS_t are the cost of electricity purchased from the grid and the revenue from the sale of electricity to the grid, respectively, ¥.

Global warming is mainly caused by CO_2 emissions from the system. The life-cycle CO_2 emissions are used as the minimum objective function [17].

Following are the emission conversion factors that can be used to calculate CO_2 emissions

$$\min T^{CD} = (E^{\mathrm{CHP}}\beta_{\mathrm{CD}}^{\mathrm{CHP}} + E^{\mathrm{B}}\beta_{\mathrm{CD}}^{\mathrm{B}} + E^{\mathrm{gidid}}\beta_{\mathrm{CD}}^{\mathrm{gid}}) \cdot l^P \tag{55}$$

Where, T^{CD} is CO_2 emissions, *kg*; E^{CHP} and E^B are the annual natural gas demand for CHP units and boilers, m^3; E^{gnd} is the annual electricity purchase for the grid, *kWh*; $\beta_{\mathrm{CD}}^{\mathrm{CHP}}, \beta_{\mathrm{CD}}^{\mathrm{B}}, \beta_{\mathrm{CD}}^{\mathrm{grid}}$ are the conversion factor for CO_2 emissions from hot spot CHP units, gas boilers, and the grid; l_p is the total number of years in the planning cycle.

Taking the number and capacity of CHP units, gas boilers, absorption chillers, wind power, storage units, and thermal storage ponds as optimization variables [18], they can be expressed as

$$\begin{aligned} V = [&CHP^{capacity}, B^{capacity}, AC^{capacity}, Wind^{capacity}, ES^{capacity}, \\ &TS^{capacity}, CHP^{number}, B^{number}, AC^{number}, Wind^{number}, \\ &ES^{number}, TS^{number}] \end{aligned} \tag{56}$$

Where, $CHP^{\mathrm{capacity}}, B^{\mathrm{capacity}}, AC^{\mathrm{capacity}}, Wind^{\mathrm{capacity}}$ are the capacity of cogeneration units, gas boilers, absorption chillers, and wind power generation, respectively, *kW*; $TS^{\mathrm{capacity}}, HS^{\mathrm{capacity}}$ are the capacity of storage devices and thermal pools, respectively, *kW•h*; CHP^{number}, B^{number}, $AC^{number}, Wind^{number}, ES^{number}, TS^{number}$ are the number of cogeneration units, gas boilers, absorption chillers, wind power generation, thermal pools, and storage devices, respectively.

3.2 Phase II Optimization Model

In the second-stage optimization model, the ultimate working fee of the device in 24 h is taken as the goal function, taking into account the price of buying electrical energy from the gadget and herbal gasoline in the course of operation, which can be expressed as

$$\min C^{\circ} = \sum_{T=1}^{24} (P_t^{\mathrm{grid}} C_{\mathrm{t}}^{\mathrm{e}} + P_t^{\mathrm{gas}} C^{\mathrm{gas}}) \Delta t \tag{57}$$

Where, C° is the daily operating cost, ¥; P_t^{grid} and P_t^{gas} are the demand of the grid and natural gas network at time *t*, *kW•h*, respectively; C_t^e is the purchased electricity cost at time *t*, ¥; C^{gas} is the purchased energy cost of natural gas, ¥; Δ_t is the simulation interval, *s*.

(a) Power balance constraint

The hourly power balance of the system can be expressed as

$$P_t^{\mathrm{CHP}} + P_t^{\mathrm{grid}} - P_t^{\mathrm{ES},c}/\eta^{\mathrm{ES,c}} + P_t^{\mathrm{Wind}} - P_t^{\mathrm{AC,cool,in}} = P_t^{\mathrm{EL}} \tag{58}$$

Where, $P_t^{\mathrm{CHP}}, P_t^{\mathrm{Wind}}$ are the output power of CHP units and wind power, *kW*; P_t^{grid} is the power purchased from the grid at time *t*, *kW•h*; $P_t^{\mathrm{ES,c}}, P_t^{\mathrm{ES,d}}$ are the charging and discharging power of electric energy storage at time *t*, *kW*; $\eta^{\mathrm{ES},c}, \eta^{\mathrm{ES},d}$ are the charging and discharging efficiency of ES; $P_t^{\mathrm{AC,cool,in}}$ is the input power of absorption chiller at time *t*, *kW*; P_t^{EL} is the electrical load demand at time *t*, *kW•h*.

The hourly thermal power balance of the system can be expressed as [19]

$$Q_t^{\mathrm{CHP}} + Q_t^{\mathrm{B}} - Q_t^{\mathrm{TS,in}}/\eta^{\mathrm{TS,in}} + \eta^{\mathrm{TS,out}} Q_t^{\mathrm{TS,out}} = Q_t^{\mathrm{HL}} \tag{59}$$

where, $Q_t^{\mathrm{CHP}}, Q_t^{\mathrm{B}}$ are the output power of the CHP unit and boiler at time *t*, *kW*, respectively; $Q_t^{\mathrm{TS,in}}, Q_t^{\mathrm{TS,out}}$ are the input and output power of the thermal storage tank at time *t*, *kW*, respectively; $\eta^{\mathrm{TS,in}}, \eta^{\mathrm{TS,out}}$ are the input and output efficiency of the thermal storage tank, Q_t^{HL} is the heat load demand at time *t*, *kW•h*.

The hourly cooling power balance of the system can be expressed as

$$Q_t^{\mathrm{AC,out}} = Q_t^{\mathrm{CL}} \tag{60}$$

Where, $Q_t^{\mathrm{AC,out}}$ is the output power of the absorption chiller at time *t*, *kW*; Q_t^{CL} is the cooling load demand at time *t*, *W•h*.

(b) Component Performance Constraints

The CHP constraint can be expressed as

$$P_m^{\mathrm{CHP,Min}} \times A_{m,t}^{\mathrm{CHP}} \le P_{m,t}^{\mathrm{CHP}} \le P_m^{\mathrm{CHP,Max}} \times A_{m,t}^{\mathrm{CHP}} \tag{61}$$

$$H_{m,t}^{\mathrm{CHP}} \le P_{m,t}^{\mathrm{CHP}} \le HPR_m \times \eta_{\mathrm{HE}} \tag{62}$$

Where, $P_i^{CHP,Min}, P_i^{CHP,Max}$ are the minimum and maximum output power of the CHP unit, *kW*; $A_{m,t}^{\mathrm{CHP}}$ is the availability of the CHP unit,

available as 1, otherwise 0; HPR_m is the heat production power of the CHP unit, *kW*; $\eta_{\mathrm{HE}}$is the heat production efficiency of the CHP unit.

The gas boiler constraint can be expressed as

$$H_{i,t}^{\mathrm{Boiler,Min}} \times A_{i,t}^{\mathrm{Boiler}} \leq H_{i,t}^{\mathrm{Boiler}} \leq H_{i}^{\mathrm{Boile,Max}} \times A_{i,t}^{\mathrm{Boiler}} \tag{63}$$

Where, $H_{i,t}^{\mathrm{Boiler,Min}}, H_{i}^{\mathrm{Boiler,Max}}$ are the minimum and maximum output power of the gas boiler, *kW*; $A_{i,t}^{\mathrm{Boiler}}$ is the availability of the gas boiler, available as 1, otherwise, it is 0.

The wind power constraint can be expressed as

$$P(v)\begin{cases} 0, & \text{if } v \leq v_{\mathrm{in}}^{c} \text{ or } v \geq v_{\mathrm{out}}^{c} \\ \dfrac{v - v_{\mathrm{in}}^{\mathrm{c}}}{v_r - v_{\mathrm{in}}^{\mathrm{c}}} P_{\mathrm{w}}^{\mathrm{r}}, & \text{if } v_{\mathrm{in}}^{c} \leq v \leq v_{\mathrm{r}} \\ P_{\mathrm{w}}^{\mathrm{r}}, & \text{if } v_{\mathrm{r}} \leq v \leq v_{\mathrm{out}}^{c} \end{cases} \tag{64}$$

Where, $v_{\mathrm{in}}^{c}, v_{\mathrm{r}}, v_{\mathrm{out}}^{c}$ are the cut-in wind speed, rated wind speed, and cut-out wind speed respectively, *m/s*. P_i^w is the rated output power *W* rate of the installed wind turbine, *kW*.

The absorption chiller can be expressed as follows:

$$Q_t^{AC,out} = COP^{AC} Q_t^{AC,in} \tag{65}$$

where COP^{AC} is the absorption chiller coefficient of performance.

The boiler constraint can be expressed as:

$$F_t^B = Q_t^B / \eta_B \tag{66}$$

Where, η_p is the boiler efficiency.

4 Improved NSGA-II Algorithm

4.1 Optimization Objectives

(a) Economical

In thinking about the economics of IES, it is vital to think about the supply side and the demand side. On the grant side, the electricity provides value including the buy price of the enter strength as properly as the operation and upkeep price of a number of sorts of equipment, whereas demand-side

economics is chiefly mirrored in users' strength buy price [20].

$$\begin{cases} f_{\mathrm{CG}} = \sum^{m} [C_{\mathrm{F}}(\boldsymbol{P}_{\mathrm{in}}(t)) + M(\boldsymbol{P}(t), |\boldsymbol{S}(t)|, \mathbf{T}(t))] \\ f_{\mathrm{CD}} = \sum_{t=1}^{m} C_{\mathrm{L}}(\boldsymbol{L}(t)) \end{cases} \tag{67}$$

Where: $f_{\mathrm{CG}}, f_{\mathrm{CD}}$ is the economics of the supply side and demand side respectively; $C_F(\bullet)$ is the external energy cost calculation function; $M(\bullet)$ is the operation and maintenance cost calculation function; $C_L(\bullet)$ is the customer energy purchase cost calculation function.

(b) Environmentality

Controlling the emission of greenhouse gases and harmful substances has always been an important issue for the energy industry and a matter of social responsibility for the operators and users of IES. It is therefore necessary to take into account the emission of pollutant gases in the energy supply process [21]. At the same time, a clean energy subsidy function is introduced to incentivize clean energy consumption.

$$\begin{cases} f_{\mathrm{EF}} = \sum_{t=1}^{m} sum(\boldsymbol{E}_{\mathrm{F}} \boldsymbol{P}(t)) \\ f_{\mathrm{CS}} = \sum_{t=1}^{m} C_{\mathrm{SUB}}(p_{\mathrm{in},t}^{\mathrm{w}}, p_{\mathrm{in},t}^{\mathrm{s}}) \end{cases} \tag{68}$$

Where: f_{EF} is gas emissions; f_{CS} is clean energy allowance; E_F is gas emission factor matrix; $C_{SUB}(\bullet)$ is the allowance calculation function.

(c) Renewable energy share target

$$\max F_{\mathrm{rec}} = \max \left(\frac{\sum_t P_{\mathrm{PV},t}}{\sum_t P_{\mathrm{CHP},t}} \right) \tag{69}$$

(d) Grid Friendliness

Time-of-use pricing can use price leverage to cut peaks and fill valleys and smooth out the load curve, thereby relaxing power constraints and reducing new capital costs [22], and this paper uses the load factor to characterize the

friendliness of the rate strategy with respect to the network.

$$f_{\mathrm{LR}} = \max\left(mean\left(\sum_{t=1}^{m} l_t\right) \Big/ \max_{t\in[1,m]} l_t \right) \tag{70}$$

The objective function of the two-stage optimization model is:

$$\begin{cases} \text{Stage 1} \begin{cases} \text{Upper Level} : \begin{cases} \min f_{\mathrm{grid}} = f_{\mathrm{CG}} - \max f_{\mathrm{CS}} \\ \min f_{\mathrm{environment}} = f_{\mathrm{EF}} \end{cases} \\ \text{Lower level} : \max \mathrm{f}_{CS} \end{cases} \\ \text{Stage 2} \begin{cases} \min f_{\mathrm{user}} = f_{\mathrm{CD}} - \max f_{\mathrm{CS}} \\ \max f_{\mathrm{comfort}} = f_{\mathrm{UC}} \\ \max f_{\mathrm{gridfriendly}} = f_{\mathrm{LR}} \end{cases} \end{cases} \tag{71}$$

4.2 Crossover Rate and Variance Adjustment Model

The model presented here for tuning the crossover rate and rate of variation of undominated individuals is an adaptive strategy based on evolutionary phases. First, the mannequin divides the evolutionary method into stages, and the beginning crossover fee and the charge of version of special tiers are constant in accordance with the adaptive approach based totally on the evolutionary stage, and the crossover price and variant fee of people in the identical evolutionary stage limit linearly with the enlarge of evolutionary generations till they are equal to the beginning crossover charge and variant price of the subsequent stage [23]; second, in order to ensure that non-dominant individuals could still participate in the late run-in phase with some Second, so that non-dominated individuals could still participate in the evolution with some probability in the latter stages of the evolution, in this model, with more evolutionary generations, both crossover rate and variation rate converge to non-zero values.

The evolutionary algorithm has a maximum crossover rate of 1 and a maximum variable rate of no more than 0.1. So that the algorithm's search process does not become a random search because of the high rate of variation, in this model, the international most crossover charge is 1.0 and the world most charge of alternate is 0.1. Searching for the choicest answer set for the hassle is a hard problem. Therefore, the variant price adjustment mannequin of non-dominated persons in the algorithm in this paper makes

use of the quantity of non-dominated men and women in the brief populace as a contrast index to measure the populace variety of the algorithm and adopts an excessive variant charge to enhance the populace diversity. This portion of a model is split into two subparts as follows.

(a) Temporary populations have fewer non-dominant individuals than permanent populations

In this case, individuals in the parent population of the next generation are dominant, and the number of non-dominance stratification is greater than 1. Therefore, population diversity enhancement is not required in this case.

Since the NSGA-II using real-number coding can have short individual gene lengths, it is straightforwardly improved by using an adaptive strategy based on evolutionary stages, this leads to the problem that the rate of variation adjustment model has an individual variation rate that is larger than the global maximum variation rate [24], for which the non-dominated individual variation rate model is divided into two cases discussed in this paper: the number of variables is not less than 10 and the number of variables is less than 10. For this subpart, the individual non-dominated cross-rate adjustment model is: In this subpart.

$$P_c \begin{cases} \dfrac{0.25(T_1 - t)}{T_1} + 0.75, & t \in [0, T_1] \\ \dfrac{0.25(T_2 - t)}{T_2 - T_1} + 0.5, & t \in (T_1, T_2] \\ \dfrac{0.5(T - t)}{(T - T_2)(1 - \beta)} + 0.5\beta, & t \in (T_2, T] \end{cases} \tag{72}$$

Variance adjustment model when the number of variables is not less than 10,

$$P_m = \begin{cases} \dfrac{\left(\min\left\{0.1, \frac{10}{L}\right\} - \frac{1}{L}\right)(T_1 - t)}{T_1} + \dfrac{1}{L}, & t \in [0, T_1] \\ \dfrac{\left(\frac{1}{L} - \frac{0.1}{L}\right)(T_2 - t)}{T_2 - T_1} + \dfrac{0.1}{L}, & t \in (T_1, T_2] \\ \dfrac{\frac{0.1}{L}(T - t)}{(T - T_2)(1 - \beta)} + \dfrac{0.1}{L}\beta, & t \in (T_2, T] \end{cases} \tag{73}$$

If the number of variables is less than 10, there are

$$P_m = \begin{cases} 0.1, & t \in [0, T_1] \\ 0.1, & t \in (T_1, T_2] \\ \dfrac{\left(0.1 - \frac{0.1}{L}\right)(T-t)}{(T-T_2)(1-\beta)} + \dfrac{0.1}{L}\beta, & t \in (T_2, T] \end{cases} \tag{74}$$

where: L is the coding length of individuals; T is the maximum number of evolutionary generations, [0, T_1] for the early stage of evolution, (T_1, T_2] for the middle stage of evolution, and (T_2, T] for the late stage of evolution; P_c is the crossover rate of non-dominated individuals, P_m is the variation rate of non-dominated individuals; $T_1 = aT$, $T_2 = (1-a)T$, usually taking $a = 0.382$ or taking $a = 0.258$; $\beta(\beta \in (0, 1])$ is the adjustment coefficient of the crossover charge and variant charge in the late evolutionary stage [25], which is set to make sure that the crossover price and variant price of non-dominated men and women are asymptotically non-zero in the late evolutionary stage and is advocated to be set to 0.4 in this paper.

(b) Among the temporary population, there are more non-dominant individuals than dominant individuals

In this case, the individuals in the parent population of the next generation are non-dominant and their stratification number of non-dominant ranks is 1. If the population diversity is increased by a high rate of variation for individuals in the population and the cross-rate adjustment model is unchanged. The rate of change adjustment model for non-dominated individuals is

$$\begin{cases} P'_m = \dfrac{P_m + P_{m\mathrm{Max}}}{2}, & N \le r < \alpha N \\ P'_m = P_{m\max}, & \alpha N \le r \le 2N \end{cases} \tag{75}$$

Where: N is the population size, the temporary population size is $2N$; r is the number of non-dominated individuals in the temporary population; $P_{mMax} = 0.1$ is the global predetermined maximum variation rate, P_m is the variation rate of non-dominated individuals before population diversity enhancement, determined by Equations (73) or (74), and P'_m is the variation rate of non-dominated individuals after population diversity enhancement; $a \in (1, 2]$ is the population diversity The recommended setting in this paper is 1.5.

In this algorithm, the pattern of adjustment of the crossover rate and variability of dominant individuals is improved by the individual-based adaptive strategy. In the improved algorithm, firstly, the cross-rate and version charge adjustment mannequin of dominant persons is set as the world's most cross-rate and version rate, and this is used as the parameter cost to run the worst-performing folks in every era of the populace [26]; then the cross-rate and variation rate is linearly assigned to dominant individuals according to the relationship between the individual stratification ordinal number and the minimum stratification ordinal number and maximum stratification ordinal number after non-dominance sorting in NSGA-II. Each individual in the dominant set linearly adjusts its own crossover rate and rate of change according to the relationship between its sorted undominated stratification ordinal number and the maximal stratification ordinal number, and the rate of crossover and rate of change of individuals in the population is modeled as follows.

$$P_c' = \frac{(P_{c\mathrm{Max}} - P_c)(i_{\mathrm{rank}} - 1)}{R - 1} + P_c \tag{76}$$

$$P_m' = \frac{(P_{m\mathrm{Max}} - P_m)(i_{\mathrm{rank}} - 1)}{R - 1} + P_m \tag{77}$$

where: P_c' is the crossover rate of dominant individuals, P_m' is the variation rate of dominant individuals, P_{cMax} is cthe rossover rate at the global level, P_{mMax} is the global maximum variation rate, *rank* is the stratification number of non-dominant sort of dominant individuals, *R* is the maximum stratification number of non-dominant sort of current population, P_c is the crossover rate of non-dominant individuals determined by Equation (72), P_m is the variation rate of non-dominated individuals determined by Equation (73) or Equation (74). In general, $P_{cMax} = 1.0$, $P_{mMax} = 0.1$.

4.3 Cross-distribution Index and Variance Distribution Index Adjustment Model

In the NSGA-II simulated binary crossover operation, the spacing of children is proportional to the spacing of parents, which is a decreasing function of the crossover distribution index η_c. The higher the value η_c, the lower the probability that the generated children are far away from the parent, and vice versa. In the polynomial variation operation, the higher the value of the variance distribution index η_m, the lower the probability of generating offspring individuals far from their parents and vice versa [27]. Therefore,

in the initial stage of NSGA-II operation, smaller η_c and η_m, should be used to make the algorithm have a greater probability of searching a more distant space and improve the algorithm's ability to explore the unknown space; with the increasing evolutionary algebra, the algorithm shifts from global search to local search and the solution individuals tend to converge, at this time, η_c and η_m, should be gradually increased to achieve a smaller range of centralized search and improve the algorithm's local search ability. Therefore, in this paper, the pass distribution index and variance distribution index of non-dominated men and women in the algorithm are adjusted by using putting the values of non-dominated people at the commencing and quit of the algorithm, and the non-dominated individuals adjust their η_c values linearly according to the evolutionary algebra during the operation of the algorithm. The model for the non-dominated individuals η_c and η_m the population is given as

$$\eta_c = \eta_{cMin} + \frac{(\eta_{cMax} - \eta_{cMin})t}{T} \tag{78}$$

$$\eta_m = \eta_{mMin} + \frac{(\eta_{mMax} - \eta_{mMin})t}{T} \tag{79}$$

Where: η_{cMin} is the cross-distribution index at the beginning of the algorithm, η_{cMax} is the across distribution index at the end of the algorithm, η_{mMin} is the variation distribution index at the beginning of the algorithm, η_{mMax} is the variation distribution index at the end of the algorithm, t is the current evolutionary generation of the population, and T is the maximum evolutionary generation. In order to make the algorithm have a large search space at the beginning of the operation and a small search space at the end of the operation, it is generally recommended $\eta_{cMin} = \eta_{mMin} = 1, \eta_{cMax} = \eta_{mMax} = 30$.

The NSGA-II algorithm flow used in this paper is shown in Figure 2 for the previously proposed mixed-integer planning problem that contains multiple objectives such as economic and environmental protection.

5 Example Analysis

5.1 System Description

In this paper, the IES composed of a 6-Bus power system and a 6-Node thermal system is the experimental object, and the standardized value parameter benchmark is 100MVA. Its system structure is shown in Figure 3. The system structure is shown in Figure 3, where: Bus 1 and Bus 2 nodes of the grid

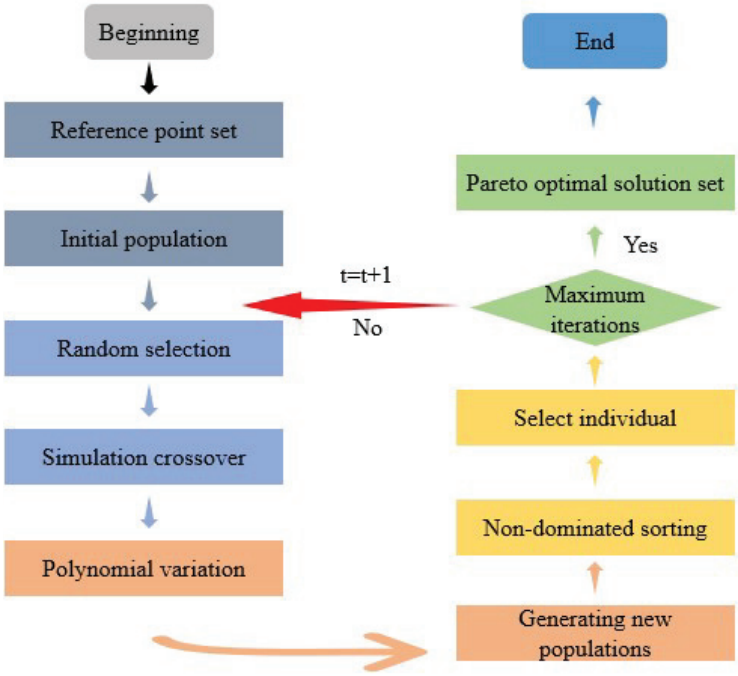

Figure 2 Flowchart of the NSGA-II algorithm.

are each connected to a DG generator set; two CHP units provide electric and thermal energy to the Bus 6 node of the grid and N 1 node of the heat network; Bus 3∼Bus 5 of the grid and N 4∼N 6 of the heat network are load nodes, and more detailed data required to describe the system are described in the literature. The system demand for electrical and thermal energy and the ambient temperature during a typical winter day 24 hours are used as experimental data sources.

According to the IES multi-objective optimal scheduling model constructed above, the effects of single-objective economic scheduling, single-objective technical dissatisfaction, economic and technical dissatisfaction, and multi-objective optimal scheduling on the optimization decision during the coordinated operation of the IES system can be compared and analyzed. Therefore, the following three cases are designed.

Case 1: Traditional single-objective economic scheduling minimizes only the economic objective F_r, without considering the system's technical dissatisfaction optimization objective.

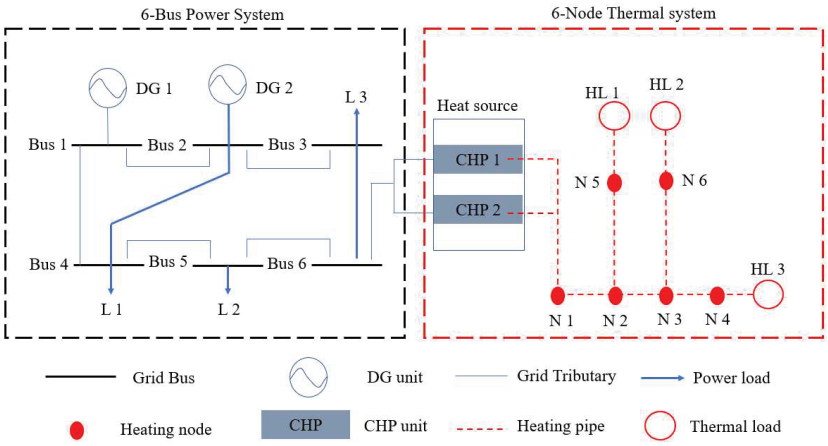

Figure 3 IES consisting of a 6-Bus electrical system and 6-Node thermal system.

Case 2: Minimizing only the system technical dissatisfaction objective F_r without considering the system economic objective.

Case 3: The Pareto the front of the multi-objective optimization hassle is solved precisely through the increased NSGA-II algorithm thinking about the device's financial and technical dissatisfaction multi-objective optimization scheduling at the identical time.

This section illustrates the effectiveness of the multi-objective optimization scheme by analyzing the optimization results of three cases.

5.2 Optimized Coordination Analysis

The NSGA-II algorithm is used to solve the two-stage multi-objective model to obtain the Pareto solution set of optimal scheduling containing 112 solutions, and the results are shown in Figures 4 and 5 shows the Pareto solution set for the economic and environmental objectives that are of most concern to the actual engineering decision makers.

As seen in Figures 4∼5, there does not exist a dispatching scheme that results in the lowest economic cost and the highest environmental friendliness of the system and the highest renewable energy share of the system. The economic and environmental objectives generally show a negative correlation, i.e., the economic cost decreases while the pollutant emissions increase.

Thus, in order to find the optimal solution further under the existing set of Pareto solutions. In this paper, we adopt the optimal solution distance method

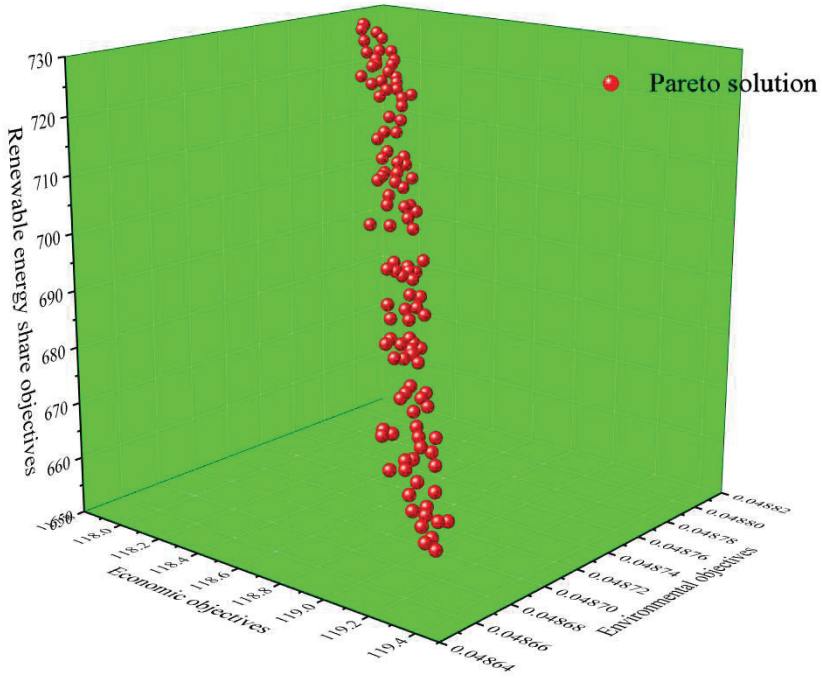

Figure 4 Three-dimensional Pareto solution set for optimal scheduling.

based on an expert evaluation to select the optimal solution based on how close a finite number of evaluation objects are to the idealized objective. One of these is the weight vector $w = (0.6, 0.3, 0.1)$ from the expert evaluation method for the three goals of economics, the share of environmental protection, and renewable energy, which comes from the decision-makers in this industrial park.

First, the optimization results of each node state variable under the above cases are analyzed. Among them, the optimization results of each power bus voltage and thermal node inlet temperature under different cases are shown in Figures 6 and 7, respectively. The critical constraints for the power bus voltage and the inlet temperature of the DHN nodes in different cases are *0.9p.u.* and *1.1p.u.* for the power bus voltage and 70°C and 90°C for the thermal node inlet temperature, respectively, but the total time that the bus voltage and the inlet temperature of (F_E^I, F_T^N) exceed the upper and lower limits of safe operation in Case 1 and Case 3 are longer than those in other cases. The total time that the total line voltage and node inlet temperature of (F_E^I, F_T^N) exceed the upper and lower limits of safe operation in both Case 1

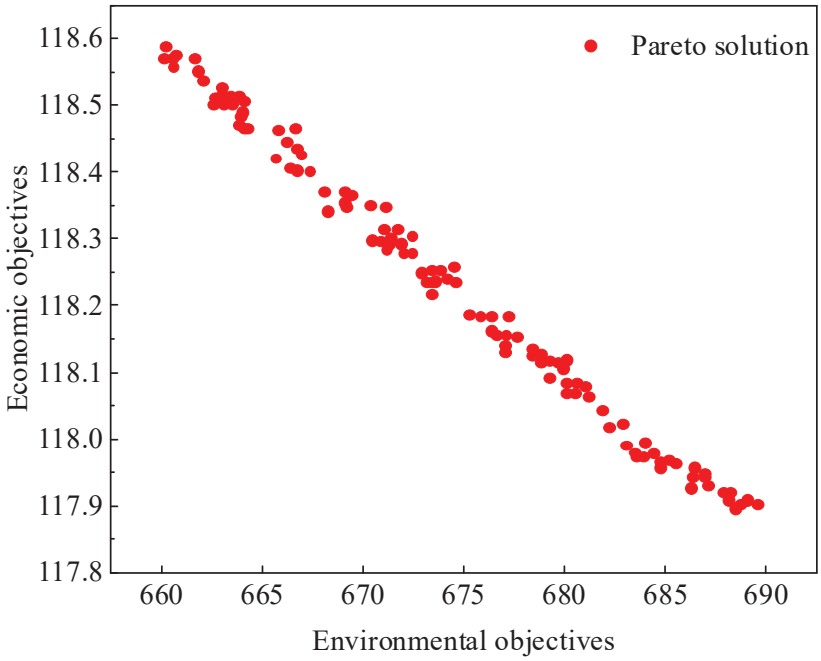

Figure 5 Pareto solution set for economic and environmental objectives.

and Case 3 exceeds the other cases. Because the optimization objective of technical dissatisfaction is considered in the IES optimal scheduling process, Case 2 and Case 3: $(F_E^N F_T^I)$ cases significantly improve the node state variables exceeding the upper and lower safe operating limits in Case 1 and Case 3: (F_E^I, F_T^N) cases, significantly improving the renewable energy of the IES system. This improvement in the node operating state comes at the cost of additional dispatching costs so decision-makers need to consider a solution for the relative tradeoff between dispatching cost and node operating state. As shown in Case 3: tradeoff solution in figure, the optimization results of its node operating state variables are between the values of Case 3: (F_E^I, F_T^N) and Case 3: $(F_E^N F_T^I)$ case node operating state variables, i.e., the simultaneous optimization of dispatching cost and technical dissatisfaction can be achieved by further adjusting the node operating state variables.

In the IES multi-objective optimal scheduling process, decision-makers also need to consider solutions for the relative trade-off between scheduling cost and technical dissatisfaction. The NSGA-II algorithm can be used to solve the complete Pareto frontier, as shown in Table 1. Among them, the

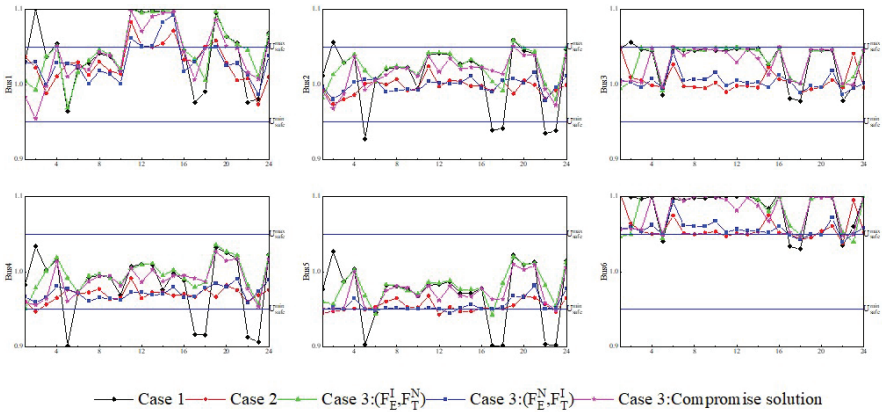

Figure 6 Voltage optimization results for each bus of the power network in different cases.

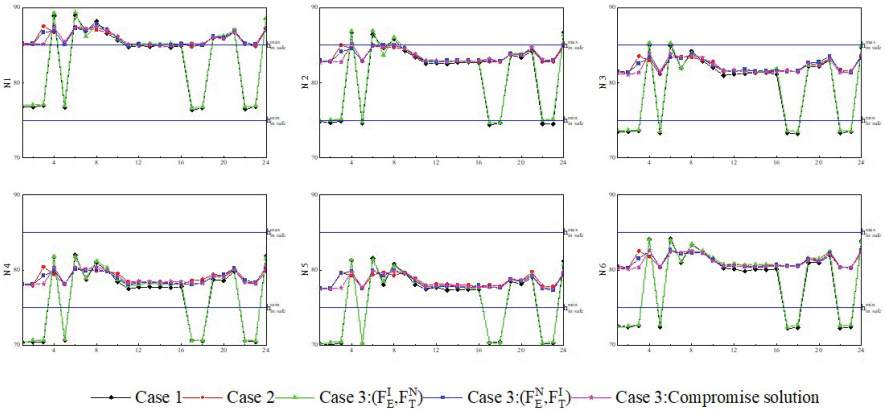

Figure 7 Optimization results of inlet temperature of each node of DHN under different cases.

points on the Pareto frontier are all optimal solutions to the IES multi-objective optimal scheduling problem, which can provide decision-makers with diverse scheduling solutions. According to the TOPSIS method, the point (30,83907.98) is determined as the best compromise solution due to the closest to the ideal point and the farthest from the negative ideal point. According to the optimization results, it can be seen that compared to the extreme point (F_E^I, F_T^N), although the scheduling cost increases by \$158.74, the technical dissatisfaction decreases by 36. Compared to the extreme point $(F_E^N F_T^I)$, although the technical dissatisfaction increases by 15, the scheduling cost decreases by \$533.75. This indicates that the obtained solution has

Table 1 Pareto frontier and optimal compromise solution for IES multi-objective optimal scheduling

Name of Each Point	Technology Dissatisfaction F_T	Economic Objectives F_E
Case 3: $(F_E^N F_T^I)$	14.8276	8.44487
Case 3: (F_E^I, F_T^N)	65.977	8.37488
Case 3: Optimal compromise solution	29.7701	8.39132
Ideal Point: (F_E^I, F_T^I)	14.9425	8.37533
Negative ideal point: $(F_E^N F_T^N)$	65.8621	8.44418
	15.7471	8.43976
	16.8966	8.43295
	20.9195	8.41445
	25.977	8.4013
	27.0115	8.39619
	30.9195	8.38961
Case 3: Pareto Frontiers	32.8736	8.38717
	33.908	8.38717
	37.0115	8.38472
	37.931	8.38423
	40.9195	8.38276
	46.8966	8.38104
	48.8506	8.3803
	52.9885	8.37858
	54.023	8.37833
	56.8966	8.37783
	57.931	8.3771
	59.7701	8.37661
	64.1379	8.37537
	65.0575	8.37488

a double benefit in terms of improving the system economy and renewable energy.

As an additional example of the applicability of the proposed method, a larger-scale IES consisting of a 33-Bus power system and an 8-Node thermal system is used for validation. Based on the stimulability results, Case 1 has a stimulability cost of $1052360, technical dissatisfaction was 862, and the mean number of iterations was 4032; In Case 2, the technical dissatisfaction is 88, the economic target is $1486177, and the average number of iterations is 4475. The NSGA-II algorithm is used to obtain the full Pareto front, where the point (240, 1093482) is determined by the TOPSIS method to be the best compromise solution to the problem. Compared to Case 1 and Case

2, the objective of technical dissatisfaction and the economic objective of this solution decreased by approximately 90% and 26 %, respectively, but the average number of iterations of the algorithm increased by 1084 and 641, respectively. 2 The results of this study are summarized in Table 1. Despite the impact of the multi-objective optimization method on computational efficiency, it still satisfies the computational time requirements of current optimal IES scheduling. These outcomes in addition confirm the effectiveness of the proposed multi-objective optimization technique and the options acquired in the equilibrium of the economy, renewable electricity, and complicated operational constraints in order to make the sure financial and steady operation of the system.

6 Conclusion

This paper investigates the IES multi-objective optimal scheduling problem and proposes a two-stage multi-objective benefit-equilibrium optimal coordination for coupled electrothermal systems, improve the NSGA-II algorithm to solve the complete Pareto frontier for this multi-objective optimization problem and use the TOPSIS method for optimal decision making. The main conclusions obtained are as follows:

(a) In this paper, we analyze the thermodynamic characteristics of each key device in the IES for electrothermal coupling, taking into account the variability of meteorological conditions and the volatility of energy supply and demand. The thermodynamic mechanism modeling of equipment, regression analysis of operational data, DOE-2 model in ASHRAE Standards 90.1, and the model based on the variability of solar radiation conditions are combined to establish the time-by-time thermodynamic modeling of each major equipment of the system under different operating the time-by-time thermodynamic characteristics of each system under different operating conditions are modeled.

(b) Based on the characteristic analysis, a two-stage multi-objective optimal configuration method is proposed to determine the optimal type, capacity, unit combination and optimal operation strategy of the multi-energy system, which optimize the total present value and CO2 emission in the planning stage and minimize the daily operation cost in the operation stage.

(c) The proposed algorithm adjusts the cross rate, variation rate, cross distribution index and variation distribution index in NSGA-II following the

traditional evolutionary stage based on individual adaptation strategy. It also gives the corresponding adaptive adjustment model, so that the algorithm can adjust the operation parameters adaptively during the evolutionary process and achieve the purpose of adaptive evolution.

(d) The model is solved by NSGA-II. The optimal Pareto solution set is obtained for the three objectives of economy, environmental protection, and renewable energy share. The weight vector of multiple objectives is $w = (0.6, 0.3, 0.1)$, and the point (240, 1093482) in the Pareto front is determined as the best compromise solution by TOPSIS method. The effectiveness of the proposed multi-objective optimization approach. The bought options, in taking into account the economics, renewable power, and complicated operational constraints, make sure the monetary and secure operation of the device, which is tested through the comparative evaluation of exclusive cases.

The case of electro-thermal coupled system studied in this paper is not equipped with a large capacity energy storage system, and with the improvement of renewable energy capacity and energy storage technology, the energy storage system plays an increasingly important role in the operation of integrated energy systems. In future research, the thermodynamic analysis and system optimization of the energy storage system can be further studied in depth.

References

[1] Wang Y, Liu C, Qin Y, et al. Synergistic planning of an integrated energy system containing hydrogen storage with the coupled use of electric-thermal energy[J]. International Journal of Hydrogen Energy, 2023.

[2] Wang L, Lin J, Dong H, et al. Demand response comprehensive incentive mechanism-based multi-time scale optimization scheduling for park integrated energy system[J]. Energy, 2023: 126893.

[3] Shi M, Wang H, Xie P, et al. Distributed Energy Scheduling for Integrated Energy System Clusters with Peer-to-Peer Energy Transaction[J]. IEEE Transactions on Smart Grid, 2022, 14(1): 142–156.

[4] Bayu A, Anteneh D, Khan B. Grid integration of hybrid energy system for distribution network[J]. Distributed Generation & Alternative Energy Journal, 2022: 667–675.

[5] Huang Zong-Hong, Cao Yu-Chen, Hu Zhi-Bing, et al. An improved genetic algorithm-based energy management method for integrated

energy systems in industrial parks [J]. Power Construction, 2019, 40(8): 51–58.

[6] Puthusserry G V, Sundareswaran K, Simon S P, et al. Maximum Energy Extraction in Partially Shaded PV Systems Using Skewed Genetic Algorithm: Computer Simulations, Experimentation and Evaluation on a 30 kW PV Power Plant[J]. Distributed Generation & Alternative Energy Journal, 2022: 1773–1796.

[7] Zhang T, Guo YT, Li YH, et al. Optimal scheduling of integrated regional energy systems with integrated electrical and thermal demand response[J]. Power System Protection and Control, 2020, 49(1): 52–61.

[8] Prakash S N, Kumarappan N. Multi-Objective Optimal Economic Dispatch of a Fuel Cell and Combined Heat and Power Based Renewable Integrated Grid Tied Micro-grid Using Whale Optimization Algorithm[J]. Distributed Generation & Alternative Energy Journal, 2022: 1433–1460.

[9] Liu Y, Zhao J, Wang L, et al. Event-Triggered Online Scheduling for Industrial-Integrated Energy System[J]. IEEE Transactions on Industrial Electronics, 2022, 70(4): 4027–4037.

[10] Wang X, Zhao R, Zhao Q, et al. Collaborative optimization of energy management in integrated energy system group based on digital twin technology[C]//2022 Power System and Green Energy Conference (PSGEC). IEEE, 2022: 435–441.

[11] Yang Hansheng. Multi-objective optimization of integrated energy system based on adaptive genetic algorithm [D]. North China University of Electric Power (Beijing), 2020.

[12] Chen Y, Deng H, Chen F, et al. Distributed Coordinated Robust Optimal Scheduling of Multi-EH-Based Integrated Energy System[C]//Proceedings of 2021 5th Chinese Conference on Swarm Intelligence and Cooperative Control. Singapore: Springer Nature Singapore, 2022: 721–732.

[13] Song Qianqian. Study on the multi-objective optimal configuration of two-layer integrated energy utilization in ecological parks [D]. Hebei Agricultural University, 2021.

[14] Tang J, Feng X, Liu J, et al. Research on multi-time scale modeling and interaction of electro-thermal coupling integrated energy system[J]. Engineering Reports, 2023: e12635.

[15] Zhang F, Wang Y, Huang D, et al. Integrated energy system region model with renewable energy and optimal control method[J]. Frontiers in Energy Research, 2022: 1766.

[16] Ge Wichun, Pan Xiao, Wang Yihe, et al. A two-stage multi-objective optimization method for integrated energy system configuration[J]. Journal of Liaoning University of Engineering and Technology (Natural Science Edition), 2020.

[17] Zhang Y, Wu X, Hu H, et al. Modeling and operation optimization of mine integrated energy system under variable conditions of typical equipment[J]. Energy Science & Engineering, 2022.

[18] Wu S, Li H, Liu Y, et al. A two-stage rolling optimization strategy for park-level integrated energy system considering multi-energy flexibility[J]. International Journal of Electrical Power & Energy Systems, 2023, 145: 108600.

[19] Xiao H, Long F, Zeng L, et al. Optimal scheduling of regionally integrated energy system considering multiple uncertainties and integrated demand response[J]. Electric Power Systems Research, 2023, 217: 109169.

[20] Jiang Yechun, Zeng Chengyu, Zhuan Jiajia, et al. Improved NSGA-II-based integrated energy multi-body benefit-balanced optimal scheduling[J]. Power Automation Equipment, 2020, 40(7): 17–23.

[21] Wang X, Li M, Chen S, et al. Optimization of Regional Integrated Energy System Cluster Based on Multi-agent Game[C]//2022 IEEE/IAS Industrial and Commercial Power System Asia (I&CPS Asia). IEEE, 2022: 533–538.

[22] Lu Q, Guo Q, Zeng W. Optimal dispatch of community integrated energy system based on Stackelberg game and integrated demand response under carbon trading mechanism[J]. Applied Thermal Engineering, 2023, 219: 119508.

[23] Wang Rongbing, Xu Hongyan, Guo Jun. Adaptive genetic algorithm for non-dominated ranking [J]. Control and Decision Making, 2018, 33(12): 2191–2196.

[24] Huang H, Liao W, Parvaneh H. Optimal Scheduling of a Residential Energy Prosumer Incorporating Renewable Energy Sources and Energy Storage Systems in a Day-ahead Energy Market[J]. Distributed Generation & Alternative Energy Journal, 2020: 265–294.

[25] Sahoo S, van Stralen J N P, Zuidema C, et al. Regionally integrated energy system detailed spatial analysis: Groningen Province case study in the northern Netherlands[J]. Energy Conversion and Management, 2023, 277: 116599.

[26] Wang Anyang, Shan Fei Fei, Zhong Wei, et al. Multi-objective optimal scheduling of integrated energy systems in industrial parks based

on non-dominated ranking genetic algorithm-III[J]. Thermal Power Generation, 2021, 50(6).

[27] Si F.Y., Han Y.H., Yuan H.T., et al. Multi-objective optimal scheduling of thermal-electric interconnected integrated energy systems with hybrid tidal constraints[J]. Control and Decision, 2021, 37(1): 97–107.

Biographies

Na Zhang received her bachelor's degree in management from Henan University of Science and Technology and is currently pursuing a master's degree in management at the School of Management, Xi'an University of Science and Technology. Her research areas include energy project management and risk management.

Taozhu Feng received his master's degree in engineering from Liaoning University of Engineering and Technology in 1994 and then worked as a master's supervisor at Xi'an University of Science and Technology, where he received the title of professor. He is a member of the China Coal Association's Economic Management Committee, a dissertation reviewer for the Ministry

of Education's Center for Academic Degrees and Postgraduate Education, a correspondence reviewer for the National Natural Science Foundation of China and the Social Science Foundation of China, and a special reviewer for the Coal Economic Research, among other things. His research areas include energy industry organization and policy, production operation and management, organizational strategy and risk management, financial management theory and practice, and human resource management.